Food Research International xxx (xxxx) 112376

Contents lists available at ScienceDirect

Food Research International

journal homepage: www.elsevier.com/locate/foodres

LC-IMS-HRMS for identification of biomarkers in untargeted metabolomics: The effects of pterostilbene and resveratrol consumption in liver steatosis, animal model

Leticia Lacalle-Bergeron [a], David Izquierdo-Sandoval [a], Alfredo Fernández-Quintela [b, c, d], María P. Portillo [b, c, d], Juan Vicente Sancho [a], Félix Hernández [a], Tania Portolés [a]

[a] Enviromental and Public Health Analytical Chemistry, Research Institute for Pesticides and Water (IUPA), Universitat Jaume I, Av. Sos Baynat S/N, 12071 Castellón de la Plana, Spain
[b] Nutrition and Obesity Group, Department of Nutrition and Food Science, Faculty of Pharmacy, University of the Basque Country (UPV/EHU), Lucio Lascaray Research Centre, 01006 Vitoria-Gasteiz, Spain
[c] BIOARABA Institute of Health, 01009 Vitoria-Gasteiz, Spain
[d] CIBERobn Physiopathology of Obesity and Nutrition, Institute of Health Carlos III (ISCIII), 01006 Vitoria-Gasteiz, Spain

ARTICLE INFO

Keywords:
Untargeted metabolomics
Ion mobility
HRMS
Resveratrol
Pterostilbene
Liver steatosis

ABSTRACT

Untargeted metabolomics with the combination of ion mobility separation coupled to high resolution mass spectrometry (IMS-HRMS) was applied to investigate the impact of resveratrol and pterostilbene supplementation on the metabolic fingerprint of the Wistar rats liver with induced liver steatosis. RP-LC and HILIC in both ionisation modes were employed to analyse the liver samples (n = 40) from Wistar rats fed with a high-fat and high-fructose diet, supplemented or not with resveratrol and pterostilbene. After univariate and multivariate statistical analysis, 34 metabolites were highlighted in the different diets and elucidated. Despite the structural similarity, different alterations in liver metabolism were observed by the supplementations. Resveratrol treatment was characterised by the alteration in metabolism of 17 lysophospholipids, while pterostilbene affected some vitamins and derivatives, among others. IMS has demonstrated great potential in the elucidation process thanks to the additional structural descriptor the CCS (Å²), providing more confidence in the identification.

1. Introduction

Foodomics is a relatively new discipline that has arisen as a result of the application of advanced analytical techniques (omics tools) and bioinformatics to nutritional and food research (Cifuentes, 2009, 2013). Among the omics tools, untargeted metabolomics (or metabolomic fingerprinting) aim to compare patterns or fingerprints of metabolites that change a biological system or state in response to endogenous (genetics, disease…) or exogenous (environment, diet…) phenomena or condition (Dettmer et al., 2007; Wolfender et al., 2015). This approach is useful to seek new biomarkers in different fields. Thus, it can provide biomarkers of diagnosis in several diseases highly prevalent in our society, such hepatic steatosis (Karu et al., 2018), characterised by the accumulation of triglycerides in the liver (Madatali Abuwani et al., 2021), biomarkers of prognosis to identify the progress of some diseases (Wang et al., 2011) like the evolution of liver steatosis to steatohepatitis or cirrhosis (Lewinska et al., 2021; Pirola & Sookoian, 2018), as well as biomarkers to characterise the effects of treatments (i.e. diet, drugs,).

Regarding treatments, an emerging working area is the study of bioactive compounds with beneficial effects on health, which are either naturally present in foodstuffs or artificially added, as in the case of functional foods. In this context, the beneficial properties of phenolic compounds, present in fruits and vegetables, have been extensively studied. Resveratrol (3,5,4′-trihydroxystilbene) is one of the most studied natural polyphenols with reported antioxidant and anti-inflammatory effects (Gimeno-Mallench et al., 2019). Nevertheless, it shows a low bioavailability due to the strong phase II metabolism that it suffers. In turn, pterostilbene is a dimethoxy derivative of resveratrol, also showing antioxidant and anti-inflammatory effects, but higher bioavailability (Kapetanovic et al., 2011; Koh et al., 2021).

A key issue of untargeted metabolomics is the characterisation of the large variety of compounds that may be involved in the subject of study in complex and diverse biological matrices (Wolfender et al., 2015). This issue can only be addressed with sufficiently sensitive and selective instruments, emphasising the hyphenation of chromatographic separations with high resolution mass spectrometry. The avail-

E-mail addresses: mariapuy.portillo@ehu.eus (M.P. Portillo), tportole@uji.es (T. Portolés).

https://doi.org/10.1016/j.foodres.2022.112376
Received 14 September 2022; Received in revised form 12 December 2022; Accepted 24 December 2022
0963-9969/© 20XX

ability of compound libraries for metabolite identification, and tools and knowledge for data analysis and interpretation are also necessary (Vivanco et al., 2011).

Liquid chromatography coupled to high resolution mass spectrometry (LC-HRMS) has been applied for untargeted metabolomics approaches in the nutrition area, for instance to reveal the metabolic changes caused by the consumption of certain foods or bioactive compounds (Fu et al., 2022; Lacalle-Bergeron et al., 2020). Firstly, liquid chromatography (LC) allows applying a wide range of separation mechanisms because of the large variety of stationary phases available. In addition, it is highly appropriate for biological matrices due to their aqueous composition, requiring less complex sample preparations for analysis than other chromatographic techniques such as gas chromatography (Segers et al., 2019). Secondly, high resolution mass spectrometry (HRMS) is the most suitable option for the detection and identification of small metabolites owing to its high sensitivity and selectivity as well as the acquisition of accurate-mass full-spectrum data (Castro-Puyana et al., 2017). Moreover, the continuous improvements in instrumentation has allowed the incorporation of ion mobility separation (IMS) to HRMS, providing an additional structural information and improving the identification process and characterisation of the biomarkers (Celma et al., 2020; Segers et al., 2019). This technique provides the collision cross section value (CCS, Å^2) of each ion, an additional characterisation parameter, based on the measurement of drift time (DT), which is dependent of the individual size, shape and charge of each ion (Mairinger et al., 2018). In addition, IMS cell layout prior to hybrid HRMS analysers allows High Definition MS^E acquisition (HDMS^E). In conventional MS^E, where accurate-mass full-spectrum at low collision energy (LE) and high collision energy (HE) are acquired simultaneously, information about the precursor ion and ion products is provided in a single injection. The incorporation of IMS data opens up the possibility to obtain cleaner fragmentation spectra without co-eluting ion fragments by filtering with the DT, as it is recorded for the precursor ion of the LE spectra and linked to its product ions in the HE spectra (Gil-Solsona et al., 2021; Paglia & Astarita, 2017).

The present work's aim was to apply an untargeted metabolomics approach, using UHPLC-IMS-HRMS, to perform a comparative study of the effects of pterostilbene and resveratrol on liver metabolome in rats suffering liver steatosis induced by a diet rich in saturated fat and fructose, as well as to explore the capabilities that the IMS brings to conventional LC-HRMS in the identification of biomarkers.

2. Materials and methods

2.1. Chemicals and reagents

The solvents methanol and acetonitrile at LC-MS grade were purchased from Scharlab (Barcelona, Spain), as well as the eluent additive formic acid for LC-MS and reagent grade ammonium acetate. HPLC-grade water was obtained with Milli-Q water purification system (Millipore Ltd., Bedford, MA, USA). Leucine-enkephalin HPLC-grade (mass-axis recalibration) and analytical standards of riboflavin, cytidine, 1-methylnicotinamide, xanthosine, asymmetric dimethylarginine and docosahexaenoic acid were purchased werewas purchased from Sigma-Aldrich (Saint Louis, MO, USA).

2.2. Animals and study Design

The experiments and animal protocols were approved by the Ethical Committee of University of the Basque Country (document reference M20_2015_245 CUEID), following the European regulations (European Convention-Strasburg 1986, Directive 2003/65/EC and Recommendation 2007/526/EC).

The study design is extensively described in Gómez-Zorita et al., 2020 (Gómez-Zorita et al., 2020). For this purpose, fifty male Wistar rats (6-week-old, 140–150 g) were housed in pairs in polycarbonate cages, after a 6-day adaptation period, under controlled conditions of temperature (22 ± 2 °C) and 12 h light–dark cycle. The rats were randomly assigned to five groups (n = 10/group): the control group (CC) was fed with a healthy balanced diet (commercial standard diet AIN-93G, OpenSource Diets, Gentofte, Denmark, D10012G); the high-fat and high-fructose group (HF) was fed with a diet containing 40 % of lipids and 22 % of fructose (OpenSource Diets, Gentofte, Denmark, D09100301), the PT15 and PT30 groups were fed with the same high-fat and high-fructose diet supplemented with pterostilbene in the amounts needed to provide doses of 15 mg/kg body weight/d (PT15 group) or 30 mg/kg body weight/d (PT30 group), and the RSV30 group was fed with the same high-fat and high-sucrose diet supplemented with resveratrol in the amount needed to provide 30 mg/kg body weight/d. During the experiment, all animals had *ad libitum* access to food and water. Food intake and body weight were recorded on a daily basis.

After the 8 weeks of experimental period, the animals underwent 12 h fasting and were sacrificed by cardiac exsanguination under anaesthesia (chloral hydrate).

2.3. Liver sampling and sample treatment

After exsanguination, livers were weighted and dissected into lobes that were individually stored at −80 °C until analysis. For this analysis, the same lobe of each liver was used.

For sample treatment, 0.5 mL of cold water:methanol (1:1) was added to ~100 mg of liver sample and manually triturated under cold conditions. Then, 0.5 mL of cold water:methanol (1:1) were added again and mixed with a Vortex for 45 min. After another 45 min in a cold ultrasound bath and centrifuging at 12,000 × rpm and a radius of 5.5 cm, 8855 g (RCF), for 30 min at 4 °C, the supernatant was divided into 3 aliquots: two vials of 300 μL were stored at −30 °C, one vial of 200 μL was stored at −80 °C. Moreover, the Quality Control sample (QC) was generated by pooling and mixing 50 μL of each sample extract.

Samples were randomly injected into the UHPLC-IMS-QTOF MS system in order to avoid the potential instrumental drift effect over the results. Assuming that QC is a representative average sample formed by a pool equivalent aliquot of all final sample extracts, it was used for both column stabilisation purposes (by 10 QC injections at the beginning of each sample batch for RP-LC and 15 for HILIC) and, following by the injection every 10 samples, to control possible instrumental drift throughout the sequence.

2.4. Instrumentation

Samples were analysed using ultra-high performance liquid chromatography (UHPLC) with a Waters ACQUITY UHPLC I-Class system (Waters, Milford, MA, USA) coupled to a VION® IMS QTof (Waters, Manchester, UK), using an electrospray ionisation interface operating in positive (ESI+) and negative (ESI−) mode. Equipment control and data acquisition and processing were performed using UNIFI software (V.1.9.2, Waters, Manchester, UK).

Two chromatographic separations were employed to cover a wider range of compound polarities. Reversed Phase Liquid chromatography (RP-LC) was used with a CORTECS® C18 fused-core 2.7 μm particle size analytical column 100 × 2.1 mm (Waters), whereas a CORTECS® HILIC fused-core 2.7 μm particle size analytical column 100 × 2.1 mm (Waters) was employed for Hydrophilic Interaction Liquid Chromatography (HILIC). For both types of liquid chromatography and both ionisation modes, gradients elution were performed at 0.3 mL/min flow rate, 40 °C column oven temperature and 1 μL sample injection volume were selected for.

The RP-LC gradient elution was performed using water (A) and methanol (B) as mobile phases, both with 0.01% of formic acid, changing as follows: 10% B at 0 min to 90% B at 14 min, 90% B at 16 min, and 10% B at 16.01 min, with a total run time of 18 min. The same gradient was employed for both ionisation modes.

For HILIC separation, mobile phases acetonitrile:water (95:5, v/v) (A) and water (B), both with 0.01 % formic acid and 10 mM ammonium acetate, were employed. The gradient started with 2 % B until 1 min, 60 % B at 10 min, 60 % B at 12 min and finally 2 % B at 12.01 min, with a total run time of 15 min. This gradient was the same for both ionisation modes.

The ESI operated at a capillary voltage of 0.7 kV and 2.00 kV for positive (ESI+) and negative (ESI−) electrospray ionisation mode, respectively. In both cases the cone voltage was 30 V, source temperature was set to 120 °C and desolvation gas to 550 °C with a flow rate of 1000 L/h. Nitrogen was used as the desolvation gas, nebulising gas, drift gas and collision gas. The mass spectrometer was operated in ion mobility ($HDMS^E$) mode for acquisition in both polarities over an *m/z* range of 50–1000 Da and a scan time of 0.3 s. In $HDMS^E$ experiments, two acquisition functions were acquired simultaneously: low-energy function (LE), with a fixed collision energy of 6 eV, and high-energy function (HE) with a collision energy ramp from 28 to 56 eV.

Calibrations of mass axis and DT were performed monthly with the "Major Mix IMS/T of calibration kit" supplied by the vendor (Waters) and Leucine-Enkephalin solution (100 μg/L acetonitrile:water (50:50, v/v) containing 0.01% formic acid) was employed for continuous recalibration of the mass axis and ensure the robust accurate mass measurement along chromatographic runs.

2.5. Data processing and statistical analysis

The raw data (*.uep*, UNIFI, Waters) were imported to Progenesis QI (V.2.5, Nonlinear Dynamics, Newcastle, UK) for baseline filter, peak alignment and other data analysis. The software automatically performs 4D peak picking (based on the intensity, *m/z*, retention time and DT), retention time alignment using QC replicates as reference (except for the first 9 QC injections used for column stabilisation in RP-LC or first 14 QC injection for HILIC); and response normalisation. The peak picking conditions were set as follows: all runs, limits (automatic), sensitivity (automatic, level 2), chromatographic peak width (minimum peak width of 0.1 min), and retention time limits (0.3 to 17 min and 0.3 to 12 min, for RP and HILIC respectively). To apply the deconvolution tool, the selected adducts ions forms $[M + H]^+$, $[M + Na]^+$, $[M + K]^+$, $[M–H_2O + H]^+$, $[2\,M + H]^+$ and $[2\,M + Na]^+$ were selected for positive ionisation analysis; and $[M–H]^-$, $[M–H_2O–H]^-$, $[M + Cl]^-$, $[M + FA\text{-}H]^-$ and $[2\,M–H]^-$ for negative ionisation analysis. Samples were originally divided into 5 groups (CC, HF, RSV, PT15 and PT30) in the "Experimental Design Setup", following the "Between-subject Design" comparison (samples from a given subject appear in only one condition). The software will then perform a One-way ANOVA calculation assuming the independence of each sample followed by a false discovery rate (FDR) optimisation approach; to test the differences among the experimental groups. The levels of statistical significance were set at 95 % level (*q-value* less than 0.05, adjusted *p*-values using the FDR approach).

The processed data were then directly exported to EZinfo (V.3.03, Umetrics, Sweden) for multivariate statistical analysis. Firstly, Principal Component Analysis (PCA), an unsupervised analysis, was applied to ensure the correct grouping of the QC replicates samples in the centre of the plot after normalisation and the absence of outliers. Then, Partial Least Square–Discriminant Analysis (PLS-DA) was conducted to maximise the separation between the groups and the validation of the model was performed by leaving-1/7-out cross-validation approach. Ultimately, an Orthogonal PLS-DA (OPLS-DA) was carried out to highlight the most robust markers (threshold $p(corr) \geq |0.6|$ and $p[1]\ loading \geq |0.1|$).

2.6. Elucidation workflow

The most significant markers highlighted in the OPLS-DA were tentatively elucidated based on their accurate masses, DT aligned HE spectra information and CCS ($Å^2$). The search in reliable mass spectra data bases as Metlin, HMDB and Lipid Maps allowed the annotation of metabolites, comparing the HE spectra to the available ones or to in-silico fragmentation spectra. In addition, CCS libraries were also employed. The final identity could only be confirmed by comparing the retention time, fragmentation and CCS with a commercially available reference standard. When the standard was not available, CCS values were predicted by means of our CCS prediction model (Bijlsma et al., 2017; Celma et al., 2022) aimed at providing additional identification confidence. Different levels of confidence in metabolite identification were employed according to Schymanski et al. (2014) classification (Schymanski et al., 2014), which was recently updated including ion mobility separation as an additional parameter for more reliable identification (Celma et al., 2020).

3. Results and discusion

3.1. Sample treatment

Regarding the sample treatment, a special care has to be taken in the pre-treatment, homogenisation and metabolite extraction stages from a tissue, in comparison with the analysis of biological fluids matrices. Firstly, to avoid metabolome changes due to temperature and enzymatic activity, more probable in tissues, the storage and transport of liver samples were kept at −80 °C until analysis. The sample treatment was performed under low temperatures as much as possible, using previously cooled solvents and employing instrumentation able to work under low temperature condition. In comparison to biological fluids as plasma or saliva, longer stages of vortex and ultrasound sonication were employed to maximise the homogenisation and to perform and exhaustive solvent-extraction of the metabolites.

A mixture of water:methanol (50:50, *v/v*) allowed to widen the polarity coverage of the metabolites, and the use of methanol in the mixture eliminated macromolecules (nucleic acids and proteins) present in the sample by deproteinisation and, thereby, allowed to focus the procedure on the low-weight molecules (metabolites). After the centrifugation to eliminate the solid residues and precipitated proteins, the resulting extract was directly injected under both LC separations (RP and HILIC) without the need for additional evaporation and redissolution in other solvents. This was possible due to the low injection volume needed (1 μL) as a consequence of the high sensitivity of the UHPLC-IMS-QTOF MS instrument. Two different LC separations were employed to detect as many compounds as possible, in positive (pos) and negative (neg) ionisation modes. RP (with a C18 column) is suited for nonpolar hydrophobic metabolites and HILIC (silica based column) for polar hydrophilic compounds. Therefore, four sample batches were performed: RP pos, RP neg, HILIC pos and HILIC neg. To avoid bias during analysis, the sample extracts were randomly injected and QC samples were injected every 10 samples for instrumental drift control and normalisation.

The data were all acquired in $HDMS^E$, where the ion mobility DT (ms) measurements are combined with the information from the LE and HE spectra acquired simultaneously, obtaining information on the precursor ion and on full-scan accurate mass fragmentation, respectively. Therefore, a 4D data was obtained at the end of the analysis, allowing to characterise each feature by the retention time from the chromatographic separation, the CCS calculated from the DT, the accurate mass and fragmentation spectra; and intensity. As the ion mobility separation

is prior to the fragmentation, the "precursor" ion shares the same DT than its fragments on the three-dimensional plots, allowing to align the feature with its fragments and to reduce the interference of co-eluting ions. Therefore, DT is useful not only as characterisation parameter but also to obtain cleaner HE spectra of near MS/MS quality, as it allows to show only the fragments that have been generated from a "precursor" ion with a given DT, and therefore, enhancing the structural elucidation (Gil-Solsona et al., 2021).

3.2. Data processing and statistical analysis

After the data import, processing with Progenesis QI starts with retention time alignment, peak picking and normalisation. All the samples were successfully aligned with a score greater than 85 % and the normalisation was performed using all compounds. The deconvolution tool allowed to group the features coming from the same compound, according to the adducts specified in the processing, and annotate them under the same label. The peak picking of the four data sets RP pos, RP neg, HILIC pos and HILIC neg resulted in the detection of 4683, 2800, 4228 and 2137 features, respectively (Supplementary data_2). Those data set were reduced to 3298, 2468, 2439 and 1437 respectively, after the removal of compounds that exhibit a poor stability with a relative standard deviation (RSD %) above 30 % within the QCs.

Multivariate unsupervised analysis PCA was then applied to each data set as exploratory visualisation of the results in order to observe trends, groupings and/or outliers. Firstly, QC replicates injected after every 10 samples (n = 9 per data set) should be clustering in the centre of the PCA score plots. Because they are a pool of all analysed samples extracts, they should act as an "average" sample and thus demonstrate by centring that the difference between the groups are not caused by instrumental drift, and therefore, indicate the correct acquisition of the data The presence of outliers was studied based on the 95 % of confidence limit of the Hotelling's T2 Range, ruling out two samples. Fig. 1 shows the PCA score plot obtained for the four data sets, where the correct clustering of QC replicates is evident in all of them, proving the proper performance of the analytical system along all, four runs. As it can be observed there is also a clear differentiation of the liver samples of rats that had been given a standard diet (CC) from those that were fed with high-fat high-fructose diet, supplemented or not with the compounds under study. This is a predictable result given that these samples were already differentiated at naked eye in the sample treatment. Given that the objective of this study was the metabolic differentiation between the livers of NAFLD-induced rats whose diets have been supplemented with pterostilbene and resveratrol, the group of CC samples were discarded for the following statistical analysis. In addition, it can be observed that PCA does not manage to clearly differentiate between resveratrol and pterostilbene supplementation from the non-supplemented samples (HF), and that the inherent differences of these samples are still too great to approach the healthy liver samples. With the 2282, 1410, 1237 and 550 statistically significant features with q-

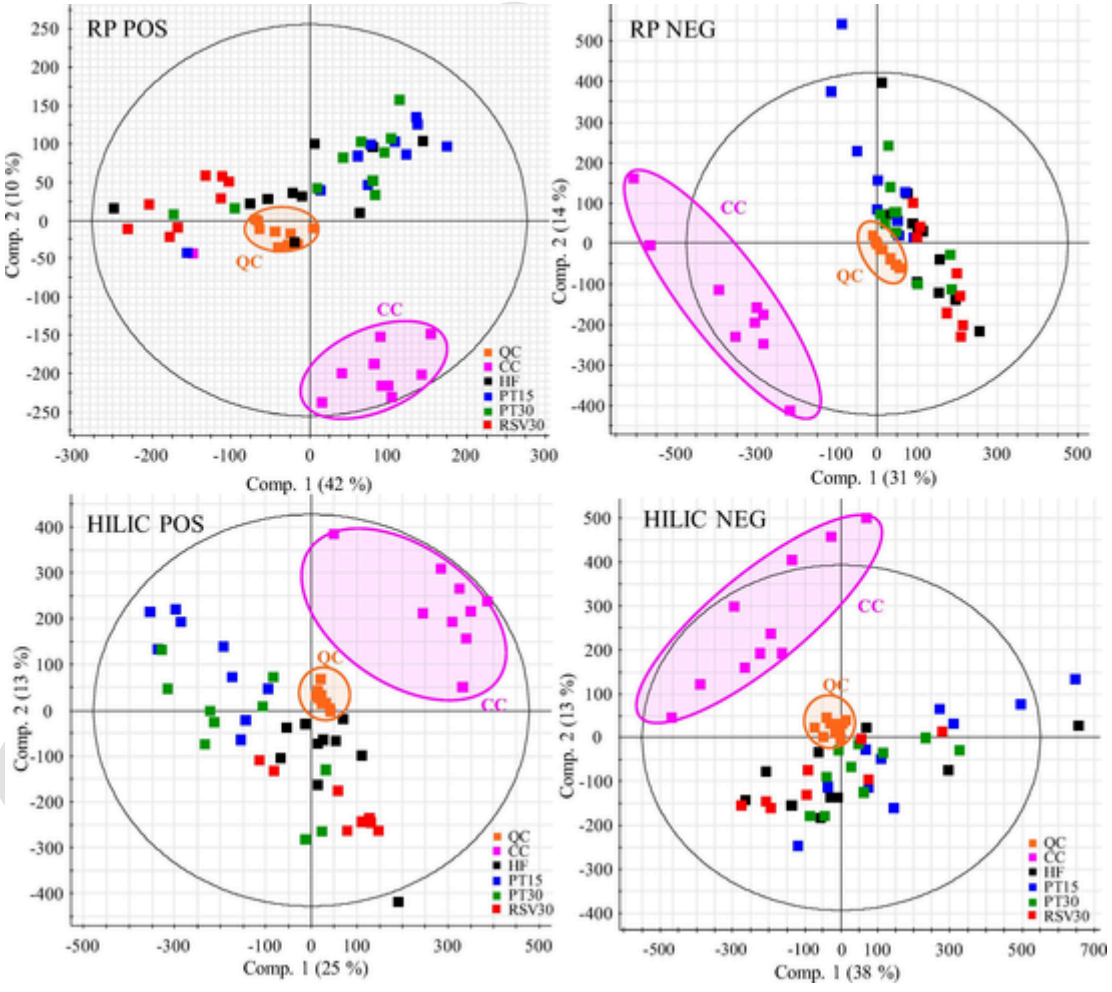

Fig. 1. PCA score plot component 1 vs component 2 for liver metabolic profiles in the four different analysis modes. The QC samples (QC ■) are grouped and centred in the plot. Five groups of liver samples from Wistar rats fed with different diets were analysed: standard diet (CC ■), high-fat and high-fructose diet (HF ■), and high-fat and high-fructose diet enhanced with 15 mg/kg/day or 30 mg/kg/day of pterostilbene (PT15 ■ and PT30 ■) or 30 mg/kg/day of resveratrol (RSV30 ■). The variance explained 79 %, 89 %, 75 % and 80 % for RP pos, RP neg, HILIC pos and HILIC neg, respectively.

value greater than 0.05 for RP pos, RP neg, HILIC pos and HILIC neg, respectively, a second PCA analysis was employed to interrogate the data. **Fig. S1** shows the PCA score plot of the first two components obtained comparing the four groups HF, PT15, PT30 and RSV30. As it can be observed, the inherent differentiation obtained by this unsupervised analysis seems to be not significant enough to clearly separate the groups, although it can be seen already a trend in the separation of RSV30 group from the others and the positioning of the HF group approximately in the centre of the graph.

Then, supervised multivariate statistical PLS-DA modelling was applied to highlight the differences between the experimental groups based on the statistically significant features. **Fig. S2** shows the PLS-DA score plot in the plane of the first two latent variables for the four data sets. The separations achieved were not ideal, obtaining coefficients for variance explained (R^2Y) from 36 to 51 % and coefficients for variance predicted (Q^2) from 18 to 40 % (Table 1). These results are close and even lower than the accepted limit of 50 % for variance explained and 40 % for predicted for biological models (Worley & Powers, 2012). This is primarily due to the low differentiation between the two dosages of pterostilbene (PT15 and PT30), demonstrating that the different dosages concentrations with pterostilbene apparently do not imply a significant variation at metabolic level. Then, it was attempted the PLS-DA differentiation considering the two dosages of pterostilbene as a single group. For the discrimination between the three resultant groups, 2457, 1388, 1325 and 557 statistically significant features were obtained for RP pos, RP neg, HILIC pos and HILIC neg, respectively. Fig. 2 shows the PLS-DA score plots obtained for the four data sets, where the differentiation has been considerably improved, obtaining R^2Y from 70 to 86 %, and Q^2 from 54 to 66 % (Table 1), resulting in 95 %, 89 %, 84 % and 84 % of the samples classified correctly for RP pos, RP neg, HILIC pos and HILIC neg, respectively. In all data sets, the first latent variable separates the two diets supplemented with pterostilbene or resveratrol (PT and RSV30); while the second component differentiated the supplemented diets from the HF group.

In order to highlight the primary features for the discrimination between the groups, an Orthogonal PLS-DA (OPLS-DA) was finally employed, where only two groups can be faced. Therefore, to highlight the most significant features three classifications were attempted by this method: HF vs RSV, HF vs PT and RSV vs PT. For all the facing, a variance explained (R^2Y) above 78 % and a variance predicted (Q^2) above 74 % were obtained, except for PT vs RSV facing in HILICpos where it was founded a $Q^2 = 58$ % (Table 2). S-Plots were generated from each OPLS-DA, allowing an easiest visualisation of the markers with higher discrimination power between the two-faced groups. From the S-plot, the most relevant ones were the features closer to *p(corr)* 1 or −1. To select the most relevant features a cut-off *p(corr)* ≥ |0.6| and *p[1] loadings* ≥ |0.1| were employed, obtaining a sum up of 117 features between the four data sets. Nevertheless, the list of possible markers was reduced still further to 34 for different reasons. For example, some of the compounds were detected more than once with the different chromatographic separation or even different polarities (e.g. feature HILICpos_2.05_376.1390n and RPpos_4.00_376.1388n both with the same CCS of 186 Å², in addition, this compound was also present in RP neg as RPneg_3.99_376.1386n). In other cases, some types of adducts or in-source fragments had not been specified in the deconvolution step of Progenesis QI, and therefore they had not been clustered and appeared as an independent feature. Finally, those features with poor signal or bad peak shape that cast doubt on their validity as markers were discarded.

Table 1
Parameters of the PLS-DA models.

Statistical model / Characteristics	PLS-DA model diagnostics							
	RP pos		RP neg		HILIC pos		HILIC neg	
Groups	4 groups PT15, PT30, RSV and HF	3 groups PT, RSV and HF	4 groups PT15, PT30, RSV and HF	3 groups PT, RSV and HF	4 groups PT15, PT30, RSV and HF	3 groups PT, RSV and HF	4 groups PT15, PT30, RSV and HF	3 groups PT, RSV and HF
Components	2	4	3	4	2	3	2	4
Variance explained R^2Y (cum)	48 %	86 %	51 %	79 %	45 %	70 %	36 %	78 %
Variance predicted Q^2 (cum)	40 %	66 %	33 %	55 %	37 %	54 %	18 %	60 %

R^2 - fit how model fits the data and Q^2 – predictive ability, by seven-round internal cross-validation as default option of EZinfo software (Umetrics, Sweden).

3.3. Elucidation process

A total of 34 markers were selected for further identification. Experimental data are recorded in **Table S1** and statistical relevance is shown in Table 3 and **Figs. S5, S6 and S7**. In order to accomplish the elucidation of those compounds, the first step was to annotate the candidates thanks to Progenesis QI identification tool, which performs a combination of neutral mass, MS/MS and CCS (if available) based searches by comparison with the $HDMS^E$ spectra and CCS data of each putative marker. The annotation of each marker was carefully reviewed based on mass accuracy and both parents and fragment ions and CCS from UNIFI raw data. Following the criteria of our laboratory and the identification level system described by Celma et al. (2020) (Celma et al., 2020), the different identification levels were given to the markers according to the data available for each of them.

Marker 1 has been selected as an illustrative example of the elucidation process followed in the present work (Fig. 3). This marker was found in HILIC pos (HILICpos_2.05_376.1390n) as marker of pterostilbene supplementation in PT vs HF (*p(corr)* 0.85) and PT vs RSV (*p(corr)* −0.74); in RP pos analysis (RPpos_4.00_376.1388n, marker of PT in PT vs HF, *p(corr)* 0.73). This maker was also present in negative mode in both RP neg (RPneg_3.99_376.1386n, marker of PT in HF vs PT) and HILIC neg with a *p(corr)* of 0.54, although below the *p(corr)* threshold applied for the selection in the latter. It is worth noticing the fact that ion mobility separation takes place prior to the fragmentation, which implies that both the parent and the fragment ions have associated the same DT. Hence, it is possible the obtaining of cleaner mass spectra without co-eluting/interfering ions when it is aligned by the DT of the parent ion. This is observed in Fig. 3**B and C** (DT filter 5.55 ± 0.22 ms, data form HILIC pos) in comparison with the unaligned ones (Fig. 3**D and E**). Therefore, it is obtained a quasi-MS^2 spectrum with composite of "product" ions obtained at different collision energies (HE energy ramp from 28 to 56 eV) pure enough and with a lot of information, which avoid the re-injection of the samples. The aligned spectra obtained from the analysis of the same ionisation modes were mostly identical (RP pos versus HILIC pos, and RP neg versus HILIC neg). Nevertheless, the unaligned spectra may give also useful information. Since the adducts are formed in the ion source previous to the ion mobility separation, $[M + Na]^+$, $[M + K]^+$ and $[M–H_2O + H]^+$ adducts DT was different enough to the protonated molecule to be aligned by DT and they can only be observed in the unaligned LE spectra (Fig. 3**D**). These adducts were all successfully deconvoluted by Progenesis QI and assigned as the same compound.

The most likely elemental composition for this marker was found to be $C_{17}H_{20}N_4O_6$ (error: +0.2, −0.01 and + 0.8 mDa in HILIC pos, RP pos and RP neg, respectively). The mean retention time across the samples in HILIC was 2.00 min and 4.00 min in RP, with a CCS of 186 Å² for the protonated and 190 Å² for the deprotonated molecule. **Fig. S3**

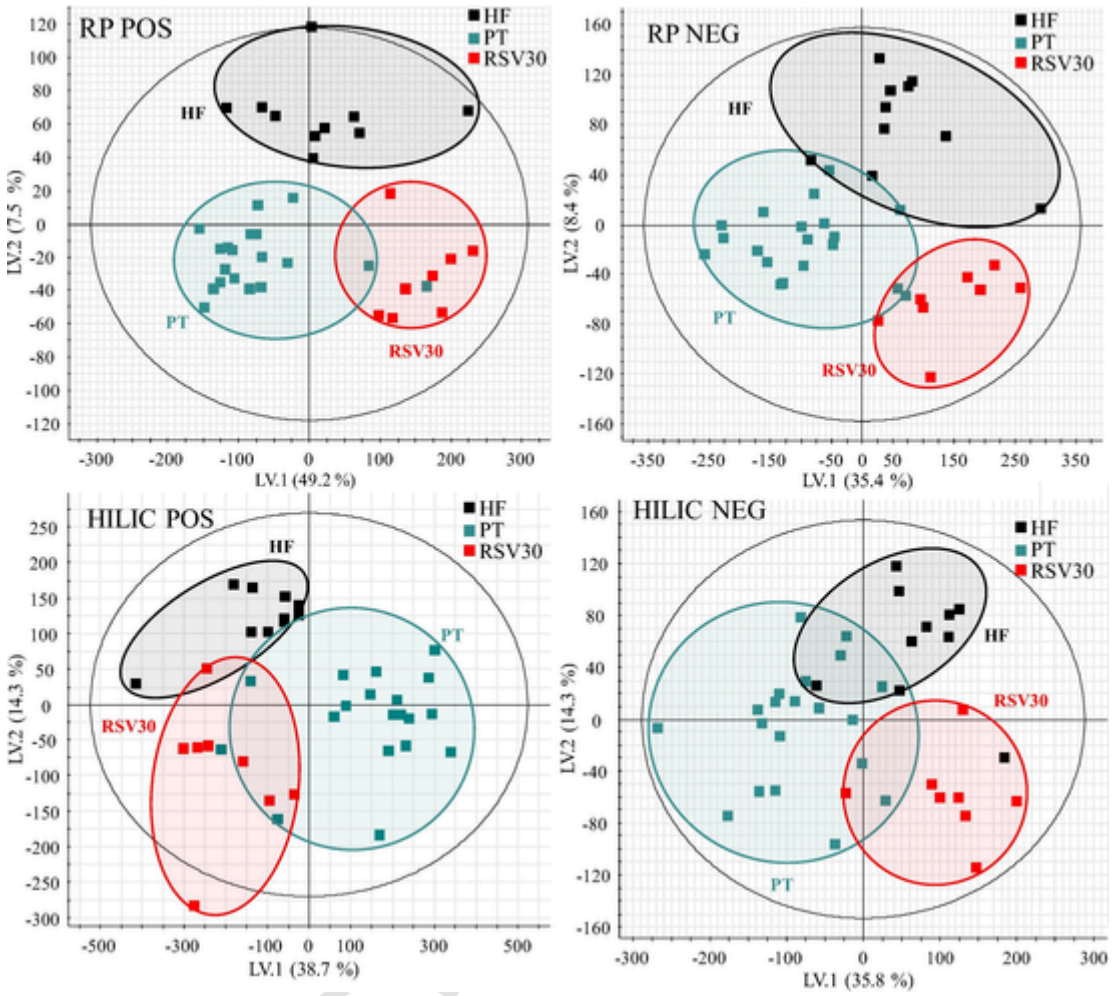

Fig. 2. PLS-DA score plot latent variable 1 vs latent variable 2 for liver metabolic profiles in the four different analysis modes. Three groups of liver samples from Wistar rats fed with different diets were analysed: high-fat and high-fructose diet (HF ■), and high-fat and high-fructose diet enhanced with 15 mg/kg/day or 30 mg/kg/day of pterostilbene (PT ■) or 30 mg/kg/day of resveratrol (RSV30 ■). Being R^2 is coefficient for variance explained and Q^2 is coefficient for variance predicted, the following results were obtained: R^2Y = 86 % and Q^2 = 66 % for RP pos, R^2Y = 79 % and Q^2 = 55% for RP neg, R^2Y = 70 % and Q^2 = 54 % for HILIC pos and R^2Y = 78 % and Q^2 = 60 % for HILIC neg.

Table 2
Parameters of the OPLS-DA models.

Statistical model / Characteristics	OPLS-DA model diagnostics											
	RP pos			RP neg			HILIC pos			HILIC neg		
	PT vs HF	RSV vs HF	PT vs HF	RSV vs HF	PT vs HF	RSV vs HF	PT vs HF	RSV vs HF	PT vs RSV	PT vs HF	RSV vs HF	PT vs RSV
	n = 20 vs 10	*n* = 10 vs 10	*n* = 20 vs 10	*n* = 10 vs 10	*n* = 20 vs 10	*n* = 10 vs 10	*n* = 20 vs 10	*n* = 10 vs 10	*n* = 20 vs 10	*n* = 20 vs 10	*n* = 10 vs 10	*n* = 20 vs 10
Components	4	6	4	6	4	6	2	4	2	3	3	2
Goodness-of-fit parameter - R^2X	77 %	90 %	77 %	90 %	77 %	90 %	60 %	87 %	59 %	89 %	64 %	54 %
Variance explained R^2Y (cum)	96 %	99 %	96 %	99 %	96 %	99 %	86 %	99 %	78 %	88 %	99 %	83 %
Variance predicted Q^2 (cum)	87 %	88 %	87 %	88 %	87 %	88 %	79 %	97 %	58 %	79 %	94 %	74 %

R^2 - fit how model fits the data and Q^2 – predictive ability, by seven-round internal cross-validation as default option of EZinfo software (Umetrics, Sweden).

shows the LE and HE DT-aligned spectra from deprotonated molecule obtained in RP neg analysis where complementary information of the elucidated structure was obtained. A proposed structure fragmentation was raised for both ionisation modes, and it was supported with the experimental spectra from METLIN with a fragmentation match over 60 % in Riboflavin (vitamin B2). Moreover, due to the availability of experimental CCS databases, this compound obtained a match with the available *Metabolic Profiling CCS Library* for Progenesis QI, with a delta error of +0.23 % (maximum CCS tolerance 2 %), increasing considerably the confidence in the Riboflavin identification.

Among the list of markers, related compounds showed similar fragmentation. Marker 9 was found in HILIC pos analysis (HILIC-

Table 3
Statistical values for the 34 markers tentatively identified.

N°	Compound	Elemental composition	*p (corr)*	Marker of	Chromatography	ESI
1	Riboflavin (Vitamin B2)	$C_{17}H_{20}N_4O_6$	0.85	PT, in HF vs PT	HILIC	pos
			−0.74	PT, in RSV vs PT		
			0.73	PT, in HF vs PT	RP	pos
			0.74	PT, in HF vs PT	RP	neg
2	Allopurinol	$C_5H_4N_4O$	0.77	PT, in HF vs PT	HILIC	pos
3	Cytidine	$C_9H_{13}N_3O_5$	−0.75	HF, in HF vs RSV	HILIC	pos
4	Methylnicotinamide	$C_7H_8N_2O$	−0.67	HF, in HF vs PT	HILIC	pos
			−0.62	HF, in HF vs RSV		
5	Nicotinamide Mononucleotide	$C_{11}H_{15}N_2O_8P$	0.70	PT, in HF vs PT	HILIC	pos
			0.67	RSV, in HF vs RSV		
6	Xanthosine	$C_{10}H_{12}N_4O_6$	−0.70	PT, in PT vs RSV	RP	neg
7	Indoleacrylic acid	$C_{11}H_9NO_2$	−0.61	HF, in HF vs PT	RP	pos
			−0.84	HF, in HF vs RSV		
8	4,5-didehydro-5-deoxyadenosine	$C_{10}H_{11}N_5O_3$	0.64	PT, in HF vs PT	HILIC	pos
			−0.65	PT, in RSV vs PT		
9	1-(a-ribofuranosyl)-lumichrome	$C_{17}H_{18}N_4O_6$	−0.76	HF, in HF vs RSV	HILIC	pos
10	Adenosine-5′-(O-methylphosphate)	$C_{11}H_{16}N_5O_7P$	0.62	RSV, in HF vs RSV	HILIC	pos
			0.73	RSV, in HF vs RSV	HILIC	neg
			0.86	PT, in HF vs PT		
			0.82	PT, in HF vs PT	RP	pos
			0.77	RSV, in HF vs RSV	RP	neg
			0.89	PT, in HF vs PT		
11	Adenosylmethionine	$C_{15}H_{22}N_6O_5S$	0.67	PT, in HF vs PT	HILIC	pos
12	ADMA (asymmetric dimethylarginine)	$C_8H_{18}N_4O_2$	−0.77	HF, in HF vs PT	HILIC	pos
13	Oxidised Glutathione	$C_{20}H_{32}N_6O_{12}S_2$	0.70	PT, in HF vs PT	HILIC	pos
			−0.62	PT, in RSV vs PT		
			−0.83	PT, in RSV vs PT	HILIC	neg
			−0.70	PT, in RSV vs PT	RP	pos
			−0.92	PT, in RSV vs PT	RP	neg
14	Resveratrol-O-sulfate	$C_{14}H_{12}O_6S$	0.82	RSV, in HF vs RSV	HILIC	neg
			0.85	RSV, in RSV vs PT		
15	Pterostilbene-4′-O-sulfate	$C_{16}H_{16}O_6S$	0.63	PT, in HF vs PT	HILIC	neg
			−0.70	PT, in RSV vs PT		
16	Docosahexaenoic acid (DHA)	$C_{22}H_{32}O_2$	0.84	RSV, in HF vs RSV	HILIC	neg
			0.71	PT, in HF vs PT		
			0.82	RSV, in HF vs RSV	RP	pos
			0.92	RSV, in HF vs RSV	RP	neg
			0.64	PT, in HF vs PT		
17	Docosapentaenoic acid (DPA)	$C_{22}H_{34}O_2$	0.80	RSV, in HF vs RSV	HILIC	neg
			0.62	PT, in HF vs PT		
			0.85	RSV, in HF vs RSV	RP	neg
			0.66	PT, in HF vs PT		
18	LysoPE(16:0)	$C_{21}H_{44}NO_7P$	0.72	RSV, in HF vs RSV	RP	neg
19	LysoPE (18:0)	$C_{23}H_{48}NO_7P$	0.81	RSV, in HF vs RSV	RP	neg
20	LysoPE(18:1)	$C_{23}H_{46}NO_7P$	0.71	RSV, in HF vs RSV	HILIC	pos
			0.69	RSV, in HF vs RSV	HILIC	neg

(*continued on next page*)

Table 3 (*continued*)

N°	Compound	Elemental composition	*p (corr)*	Marker of	Chromatography	ESI
21	LysoPE(18:2)	$C_{23}H_{44}NO_7P$	0.71	RSV, in HF vs RSV	HILIC	neg
22	LysoPE(20:4)	$C_{25}H_{44}NO_7P$	0.86	RSV, in HF vs RSV	HILIC	pos
			0.88	RSV, in PT vs RSV		
			0.69	RSV, in HF vs RSV	HILIC	neg
			0.69	RSV, in PT vs RSV	RP	neg
23	LysoPE(22:6)	$C_{27}H_{44}NO_7P$	0.88	RSV, in HF vs RSV	HILIC	pos
			0.72	RSV, in HF vs RSV	HILIC	neg
24	LysoPC(16:0)	$C_{24}H_{50}NO_7P$	0.84	RSV, in HF vs RSV	HILIC	pos
			0.92	RSV, in PT vs RSV		
			0.74	RSV, in HF vs RSV	RP	pos
25	LysoPC(18:1) isomer 1	$C_{26}H_{52}NO_7P$	0.88	RSV, in PT vs RSV	HILIC	pos
26	LysoPC(18:1) isomer 2	$C_{26}H_{52}NO_7P$	0.82	RSV, in HF vs RSV	HILIC	pos
			0.92	RSV, in PT vs RSV		
27	LysoPC(18:3)	$C_{26}H_{48}NO_7P$	0.78	RSV, in HF vs RSV	HILIC	pos
			0.88	RSV, in PT vs RSV		
28	LysoPC(20:4) isomer 1	$C_{28}H_{50}NO_7P$	0.75	RSV, in PT vs RSV	HILIC	pos
29	LysoPC(20:4) isomer 2	$C_{28}H_{50}NO_7P$	0.72	RSV, in PT vs RSV	HILIC	pos
30	LysoPC(22:6)	$C_{30}H_{50}NO_7P$	0.74	RSV, in PT vs RSV	HILIC	pos
31	LysoPI(20:4)	$C_{29}H_{49}O_{12}P$	0.81	RSV, in HF vs RSV	HILIC	neg
32	LysoPS(20:4)	$C_{26}H_{44}NO_9P$	0.91	RSV, in HF vs RSV	HILIC	neg
33	LysoPS (21:0)	$C_{27}H_{54}NO_9P$	0.87	RSV, in HF vs RSV	RP	neg
34	LysoPS (2-OMe-18:0)	$C_{25}H_{52}NO_9P$	0.78	RSV, in HF vs RSV	RP	neg
			0.90	RSV, in HF vs RSV		

pos_1.28_375.1304 *m/z*) as marker of high-fructose high-fat diet (HF group) in RSV vs HF (*p(corr)* −0.76), obtaining a level 3 tentative elucidation as 1-(a-ribofuranosyl)-lumichrome with molecular formula $C_{17}H_{18}N_4O_6$ (see marker structure in **Fig. S4**). This marker shared with riboflavin the non-specific water loss (*m/z* 357.1182, −1.69 mDa), and fragments *m/z* 243.0882 ($[C_{12}H_{11}N_4O_2]^+$, −0.0 mDa), *m/z* 198.0664 ($[C_{11}H_8N_3O]^+$, −0.3 mDa) and *m/z* 172.0868 ($[C_{10}H_{10}N_3O]^+$, −0.7 mDa) observed in the DT aligned HE spectra of riboflavin (Fig. 3**C**), which shows that they share in their structure the nitrogenous base flavin.

Markers 8, 10 and 11, tentatively elucidated as 4,5-didehydro-5-deoxyadenosine, adenosine-5′-(O-methylphosphate) and adenosylmethionine, respectively, shared the same fragment *m/z* 136.0619 ($[C_5H_6N_5O]^+$, −0.5 mDa) in positive ionisation mode, corresponding to the adenosine base shared by all of them.

But the clearest example of similar behaviour in fragmentation occurs in 17 lysophospholipids tentatively elucidated. This type of compounds is made up of a glycerol molecule to which a fatty acid and phosphate group are bind. Phosphate is attached via phosphodiester bond to other molecules, such as ethanolamine (LysoPE), choline (LysoPC), inositol (LysoPI) or serine (LysoPS). Due to the large number of isomers in this type of molecules (because of the double bond position, position of fatty acid attachment to the glycerol molecule or number of unsaturations) it is troublesome to give a definitive identification with the data acquired for most of them. It is also difficult to obtain fragments that give clues about the unsaturation position in the fatty acid chain. Hence, the elucidation is mostly based on the common fragmentation spectra for the different types of lysophospholipids as well as the molecular formula to define the number of carbons and the unsaturations of the attached fatty acid. LysoPE can be observed in both positive and negative ionisation, and the fragmentation is characterised by neutral loss of phosphoethalonamine group (Δ*m/z* 141. 0191) in positive ionisation mode and fragments *m/z* 196.0375 and *m/z* 140.0119 in negative ionisation mode. LysoPC are typically observed in positive ionisation mode and shared fragments *m/z* 184.0740 and *m/z* 104.1075 corresponding phosphocholine and choline fragments. Regarding LysoPI and LysoPS, they were mainly observed in negative ionisation mode. In DT aligned HE spectrum of marker 31 LysoPI(20:4) it 4 typical ions recorded for this class of phospholipids were observed: *m/z* 152.9949 ($[C_3H_6O_5P]^-$, −0.4 mDa) and *m/z* 241.0108 ($[C_6H_{10}O_8P]^-$, −0.5 mDa) coming from the phosphoinositol group, as well as the fragments coming from the fatty acid attached *m/z* 259.2419 ($[C_{19}H_{31}]^-$, −0.7 mDa) and *m/z* 303.2315 ($[C_{20}H_{31}O_2]^-$, −0.4 mDa). Finally, LysoPS presented the neutral loss of serine group (Δ*m/z* 87.0320). For 7 of the lysophospholipids, a match with CCS experimental data base were obtained, with a delta error of + 2.3 %, +1.3 %, +1.6 % for deprotonated molecules of LysoPE(16:0), LysoPE(20:4) and LysoPE(22:6) respectively; and + 0.1 % and −2.4 % for protonated molecules of both isomers of LysoPC (18:1) and both isomers of LysoPC(20:4) respectively.

In order to achieve more confidence in tentative identification, it was employed a CCS predictor model based on Multiple Adaptative Regression Splines (MARS) developed for Travelling Wave Ion mobility instrument (TWIMS) (VION®, Waters) (Celma et al., 2022). The relative errors obtained with this prediction tool were below ±4.05 % for protonated ion and ±5.86 % for deprotonated molecules for 95% of all CCS values tested. This predictor was applied from marker 1 to 17 without a match with experimental CCS (see **Table S1**). For markers from 1 to 13 and fatty acids markers 16 and 17 without match with experimental CCS library, delta CCS errors ranging from 0.1 to 1.5 % for protonated ion and 0.1 to 1.9 % for deprotonated ion, increased the confidence of the identification. The only exception was docosahexaenoic acid with a delta error of −3.9 % for protonated molecule, while the data for deprotonated molecule was less than 1 %.

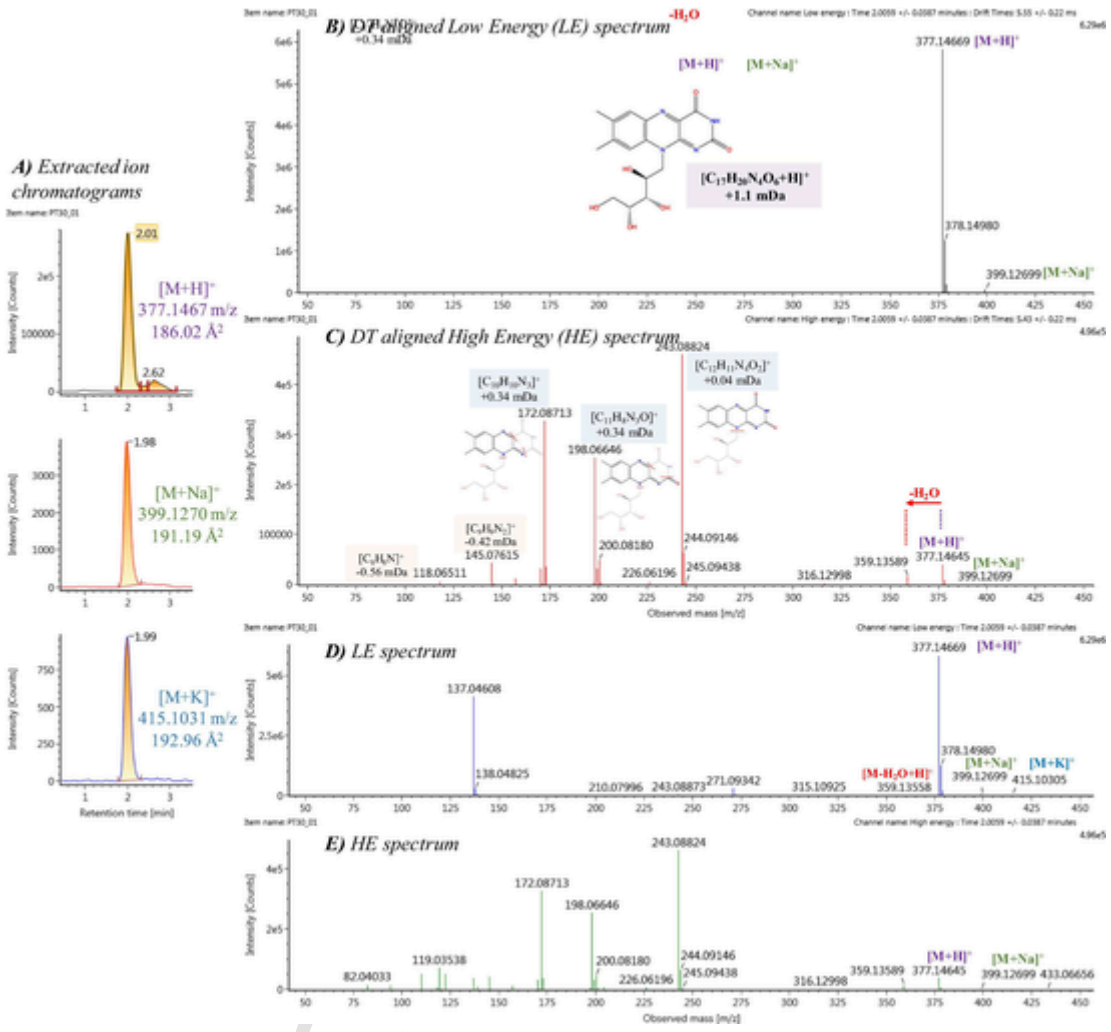

Fig. 3. Elucidation of marker 1 Riboflavin (vitamin B2) based in chromatograms and HDMS^E spectra obtained from HILIC pos analysis: **A**) Extracted ion chromatograms of adducts found, along with the experimental *m/z* and CCS, **B**) DT aligned LE spectrum, **C**) DT aligned HE spectrum, **D**) LE spectrum and **E**) HE spectrum. A structure fragmentation is proposed.

The higher delta error obtained for phase II sulphate conjugated metabolites (-4.5 % and −7.9 % for sulphated metabolite form resveratrol and pterostilbene, respectively) can be explained by the absence of these family of compounds during the building of the CCS prediction model. The low commercial availability of pure analytical standards of these compounds makes difficult to obtain experimental CCS information to be included in the building of the prediction tool.

For phospholipids, a more specialised prediction tool was employed: LipidCCS CCS prediction model Zhou et al. (2017). This prediction model achieved median relative errors (MRE) of ~1%, from the CCS information obtained from a large set of lipids measured with Drift Tube Ion Mobility instruments (DTIMS). For, Travelling Wave Ion Mobility instruments (TWIMS) as VION® employing polyAla calibrants are used the MRE increased to ~4%. Actually, if these error outputs (MRE = 50 % confidence interval) are given within a confidence interval of 95 %, the errors for DTIMS instruments will be closer to ±3 % and higher for TWIMS instruments with polyAla calibrants. PolyAla calibrants has been shown to have a considerable impact in lipids CCS errors (George et al., 2022; Hines et al., 2016), unfortunately the instrument employed do not allowed us to employ a more specialised calibrant. Nevertheless, it was employed this Lipid CCS instead of the in-house prediction model due to the lack of phospholipids experimental data in its building.

For markers from 18 to 34 without a match with experimental CCS library, predicted CCS with delta errors ranging from 0.6 to 5.4 % for protonated ions and 1.7 to 8.3 % for deprotonated ions were obtained. The lysoPS markers led to a poor prediction, with delta error from 5.1 to 8.3 % for their deprotonated ions. Moreover, due to the difficulty to find pure standards for isomeric lipid to train the model, LipidCCS could not accurately differentiate between isomers. Although, trans lipids are not usually observed as endogenous lipids, and therefor it is not a big issue that LipidCCS can not differentiate between position geometry (cis/trans). Therefore, a more precise identity of these compounds could not be reached with the information obtained.

All the work described so far, shows the interesting information that ion mobility separation offers to untargeted metabolomics studies, improving the time-consuming identification step, still the main bottleneck in the metabolomics workflow. CCS is an additional structural descriptor highly reproducible and mostly transversal between instruments, opposite to retention time, which depends on chromatographic separation and can be heavily influenced by sample matrix. For this reason, there is a trend to include CCS values among the experimental data in compound databases and, in turn, predictive tools of great interest are increasingly being created and implemented.

The unequivocally confirmation of the identity of the markers (identification level 1) can only be reached by comparison with a reference standard. This level could be obtained for six markers: marker 1 riboflavin, marker 3 cytidine, marker 4 methylnicotinamide, marker 6 xanthosine, marker 12 ADMA, marker 13 oxidised glutathione and

marker 16 docosahexaenoic acid. For marker 2, two potential isomeric compounds were plausible, hypoxanthine and allopurinol. The standard of hypoxanthine was purchased but it did not match with in terms of retention time. Therefore, hypoxanthine was discarded, and allopurinol was assumed as tentative identification for this marker (level 2b) until definitive confirmation with its corresponding analytical standard.

3.4. Changes in liver metabolome

The untargeted analysis performed showed three clearly differentiated metabolome profiles: 1) rats fed with the high-fat and high-fructose diet (HF group), 2) rats fed with the same diet and treated with pterostilbene, and 3) rats fed with the same diet and treated with resveratrol. This confirms that the methodology applied was appropriate to seek biomarkers of treatment and to characterise the effects of the two phenolic compounds used in the present study. In **Figs. 4, 5 and 6**, the mean abundances of the highlighted markers in PT vs HF, RSV vs HF and PT vs RSV are shown, respectively. These figures allow to observe the differences in intensity for each marker between the two groups compared. Since the markers were detected in different analysis and with different ionisation modes, the intensities obtained are not comparable between markers (i.e. a greater intensity of a marker does not necessarily imply higher concentration than another marker with lower intensity). For those markers detected in different analysis, the figures show the normalised abundance coming from the analysis with higher statistical relevance. Supplementary Figs. S5–S8 show in detail the variation in the intensity obtained across the groups of samples for each marker.

Resveratrol is a polyphenol, belonging to the group of stilbenes and pterostilbene is its dimethoxy derivative. The present study shows a clear different effect of pterostilbene and resveratrol on hepatic metabolite profile, despite of their similarity in terms of chemical structure. Firstly, although the phase II sulphated metabolites of each compound were found as marker of their respective groups, a considerable difference could be observed between the supplementation of 15 mg/kg/d and 30 mg/kg/d of pterostilbene for pterostilbene-4-O-sulfate (**Fig. S6**). When the rats fed with the high-fat and high-fructose diet were treated with pterostilbene (Fig. 3), significant changes were observed in three vitamins and derivatives (marker 1 riboflavin, marker 4 methylnicotinamide and marker 5 nicotinamide mononucleotide), four nucleotides/nucleosides (marker 2 allopurinol, marker 6 xanthosine, marker 8 4,5-didehydro-5-deoxyadenosine and marker 10 adenosine-5′-(o-methylphosfate)), three peptides/amino acids (marker 11 adenosylmethionine, marker 12 asymmetric dimethylarginine and marker 13 oxidised glutathione), and three organic acids (marker 16 docosahexaenoic acid, marker 17 docosapentaenoic acid and marker 7 indoleacrylic acid). On the other hand, for rats treated with resveratrol (**Fig. 4**), the changes affected to vitamin-related compound (increased levels of marker 5 nicotinamide mononucleotide and decreased level of marker 9 1-(a-ribofuranosyl)-lumichrome and marker 4 methylnicotinamide), nucleotides/nucleosides ratio (higher level of marker 10 adenosine-5′-(o-methylphosfate) and lower of marker 3 cytidine), three organic acids (marker 16 docosahexaenoic acid, marker 17 docosapentaenoic acid and marker 7 indoleacrylic acid) and seventeen phospholipids. In a reduced number of cases, both phenolic compounds induced similar changes in the same metabolites in comparison with HF group: decreased levels of cytidine, methylnicotinamide and indoleacrylic acid, and increased levels in nicotinamide mononucleotide, adenosine-5′-(o-methylphosphate), docosapentaenoic acid (DPA) and docosahexaenoic acid (DHA). The positive effects in different liver-related diseases have been already reported with regard to the presence/increase of DPA and DHA (Enguita et al., 2019) as well as, nicotinamide mononucleotide (Zong et al., 2021).

Regarding the rats treated with pterostilbene, it was interesting the decrease in asymmetric dimethylarginine (ADMA) and the increase in s-adenosylmethionine (SAM), in comparison to the group without supplementation (HF). ADMA, an endogenous inhibitor of nitric oxide synthase, is formed by methylation of arginine residues in proteins. In this process, SAM, which is mainly synthesised and consumed in the liver, is the methyl donor. ADMA mediates its adverse vascular effects by impairing endothelial, nitric oxide-dependent function, which leads to decreased vasodilatation, increased smooth muscle cell proliferation, platelet dysfunction and increased monocyte adhesion (Maas, 2005). Moreover, it has been reported that SAM is able to ameliorate lipid accumulation and oxidative stress in hepatic cells, mainly through promoting mitochondrial fatty acid entry for β-oxidation and external triglyceride release (Vergani et al., 2020). These results on the positive effect of supplementation with pterostilbene are encouraging, since the reduction in ADMA values are associated with various clinical settings as coronary heart disease, hypertension and diabetes among others, and at the same time it is increased the presence of SAM and its possible protection against the free radical toxicity.

In the case of the rats treated with resveratrol, the main changes took place in phospholipids. These molecules can be precursors of lipid mediators, which play important roles in external and internal communication and modulate cellular responses. Previous studies have demonstrated a reduction in phosphatidylcholine (PC) among other phospholipids in non-alcoholic fatty liver disease (NAFLD) patients (Piras et al., 2021), therefore it is promising that resveratrol supplementation increases the levels of these compounds.

The present study may help to generate new hypothesis about the preventive effects of pterostilbene and its parent compound, by indicating potential pathways to be addressed in an ongoing study.

4. Conclusions

The great potential of the inclusion of IMS into the conventional LC-HRMS for untargeted metabolomic studies has been demonstrated with the tentative elucidation of 34 markers related to the treatment with resveratrol and pterostilbene to rats with liver showing steatosis. Markers identified were 2 phase II sulphated metabolites, 17 lysophospholipids, 3 fatty acids, 4 vitamin and related compounds, 5 nucleosides/nucleotides and 3 peptide/amino acids related compounds. The implementation of CCS as additional molecular descriptor and the tools created around this parameter facilitated the compound identification, helping to solve the bottleneck that the elucidation process represents in untargeted metabolomics. Significantly different results have been obtained for the two types of supplementation despite the similarity between both phenolic compounds (resveratrol and pterostilbene).

Currently, a parallel work focused on the markers found in this work is being carried out. The objective is to investigate the implication of the highlighted metabolites in stopping the progression of liver steatosis to more severe pathologies and evaluate the metabolic pathways altered.

CRediT authorship contribution statement

Leticia Lacalle-Bergeron : Conceptualization, Methodology, Software, Validation, Formal analysis, Investigation, Resources, Data curation, Writing – original draft, Writing – review & editing, Visualization. **David Izquierdo-Sandoval :** Conceptualization, Methodology, Software, Validation, Formal analysis, Investigation, Resources, Data curation, Writing – review & editing. **Alfredo Fernández-Quintela :** Conceptualization, Investigation, Resources, Writing – review & editing, Supervision, Project administration, Funding acquisition. **María P. Portillo :** Conceptualization, Investigation, Resources, Writing – review & editing, Supervision, Project administration, Funding ac-

quisition. **Juan Vicente Sancho :** Conceptualization, Methodology, Validation, Investigation, Resources, Data curation, Writing – review & editing, Visualization, Supervision, Project administration, Funding acquisition. **Félix Hernández :** Conceptualization, Methodology, Investigation, Resources, Writing – review & editing, Supervision, Project administration, Funding acquisition. **Tania Portolés :** Conceptualization, Methodology, Software, Validation, Investigation, Resources, Data curation, Writing – review & editing, Visualization, Supervision, Project administration, Funding acquisition.

Declaration of Competing Interest

The authors declare that they have no known competing financial interests or personal relationships that could have appeared to influence the work reported in this paper.

Acknowledgements

L Lacalle-Bergeron acknowledges the financial support of Universitat Jaume I, Spain for his pre-doctoral grant (UJI 19I001/03). D. Izquierdo-Sandoval acknowledges the Ministry of Science, Innovation and Universities of Spain for funding his research through the FPU predoctoral program (FPU19/ 01839). T. Portoles acknowledges Ramon y Cajal Program from the Ministry of Economy and Competitiveness, Spain (RYC-2017-22525) for funding her research. The Research Institute for Pesticides and Water (IUPA) authors acknowledge the financial support of Generalitat Valenciana, as research group of excellence PROMETEO/2019/040 and Universitat Jaume I de Castelló (UJI-B2020-25 and UJI-B2020-37). The Nutrition and Obesity Group acknowledge the financial support of the University of the Basque Country, as a research group of excellence (GIU 18/173), the *Ministerio de Economía y Competitividad-Fondo Europeo de Desarrollo Regional*, grant number AGL-2015-65719-R MINECO/FEDER, UE) and CIBERobn, grant number CB12/03/30007.

Appendix A. Supplementary material

Supplementary data to this article can be found online at https://doi.org/10.1016/j.foodres.2022.112376.

References

Bijlsma, L., Bade, R., Celma, A., Mullin, L., Cleland, G., Stead, S., … Sancho, J.V. (2017). *Prediction of collision cross-section values for small molecules: Application to pesticide residue analysis*. *Analytical Chemistry*, *89*(12), 6583–6589. https://doi.org/10.1021/acs.analchem.7b00741.

Castro-Puyana, M., Pérez-Míguez, R., Montero, L., & Herrero, M. (2017). *Application of mass spectrometry-based metabolomics approaches for food safety, quality and traceability*. *TrAC Trends in Analytical Chemistry*, *93*, 102–118. https://doi.org/10.1016/j.trac.2017.05.004.

Celma, A., Bade, R., Sancho, J.V., Hernandez, F., Humphries, M., & Bijlsma, L. (2022). *Prediction of retention time and collision cross section (CCS H+, CCS H–, and CCS Na+) of emerging contaminants using multiple adaptive regression splines*. *Journal of Chemical Information and Modeling*, *1–16*. https://doi.org/10.1021/acs.jcim.2c00847.

Celma, A., Sancho, J.V., Schymanski, E.L., Fabregat-Safont, D., Ibáñez, M., Goshawk, J., … Bijlsma, L. (2020). *Improving target and suspect screening high-resolution mass spectrometry workflows in environmental analysis by ion mobility separation*. *Environmental Science and Technology*. https://doi.org/10.1021/acs.est.0c05713.

Cifuentes, A. (2009). *Food analysis and foodomics*. *Journal of Chromatography A*, *1216*(43), 7109. https://doi.org/10.1016/j.chroma.2009.09.018.

Cifuentes, A. (2013). Foodomics: principles and applications. In A. Cifuentes (Ed.), *Foodomics: advanced mass spectrometry in modern food sciences and nutrition* (p. 580). John Wiley & Sons, Inc. <https://www.wiley.com/en-us/Foodomics%3A+Advanced+Mass+Spectrometry+in+Modern+Food+Science+and+Nutrition-p-9781118169452>.

Dettmer, K., Aronov, P.A., & Hammock, B.D. (2007). *Mass spectrometry-based metabolomics*. *Mass Spectrometry Reviews*, *26*(1), 51–78. https://doi.org/10.1002/mas.20108.

Enguita, M., Razquin, N., Pamplona, R., Quiroga, J., Prieto, J., & Fortes, P. (2019). *The cirrhotic liver is depleted of docosahexaenoic acid (DHA), a key modulator of NF-κB and TGFβ pathways in hepatic stellate cells*. *Cell Death & Disease*, *10*(1), 14. https://doi.org/10.1038/s41419-018-1243-0.

Fu, J., Zhang, L.-L., Li, W., Zhang, Y., Zhang, Y., Liu, F., & Zou, L. (2022). *Application of metabolomics for revealing the interventional effects of functional foods on metabolic diseases*. *Food Chemistry*, *367*(April 2021), 130697. https://doi.org/10.1016/j.foodchem.2021.130697.

George, A.C., Schmitz-Afonso, I., Marie, V., Colsch, B., Fenaille, F., Afonso, C., & Loutelier-Bourhis, C. (2022). *A re-calibration procedure for interoperable lipid collision cross section values measured by traveling wave ion mobility spectrometry*. *Analytica Chimica Acta*, *1226*(July), 340236. https://doi.org/10.1016/j.aca.2022.340236.

Gil-Solsona, R., Sancho, J.V., Gassner, A., Weyermann, C., Hernández, F., Delémont, O., & Bijlsma, L. (2021). *Use of ion mobility-high resolution mass spectrometry in metabolomics studies to provide near MS/MS quality data in a single injection*. *Journal of Mass Spectrometry*, *56*(5). https://doi.org/10.1002/jms.4718.

Gimeno-Mallench, L., Mas-Bargues, C., Inglés, M., Olaso, G., Borras, C., Gambini, J., & Vina, J. (2019). *Resveratrol shifts energy metabolism to increase lipid oxidation in healthy old mice*. *Biomedicine & Pharmacotherapy*, *118*(March), 109130. https://doi.org/10.1016/j.biopha.2019.109130.

Gómez-Zorita, S., González-Arceo, M., Trepiana, J., Aguirre, L., Crujeiras, A.B., Irles, E., … Portillo, M.P. (2020). *Comparative effects of pterostilbene and its parent compound resveratrol on oxidative stress and inflammation in steatohepatitis induced by high-fat high-fructose feeding*. *Antioxidants*, *9*(11), 1042. https://doi.org/10.3390/antiox9111042.

Hines, K.M., May, J.C., McLean, J.A., & Xu, L. (2016). *Evaluation of collision cross section calibrants for structural analysis of lipids by traveling wave ion mobility-mass spectrometry*. *Analytical Chemistry*, *88*(14), 7329–7336. https://doi.org/10.1021/acs.analchem.6b01728.

Kapetanovic, I.M., Muzzio, M., Huang, Z., Thompson, T.N., & McCormick, D.L. (2011). *Pharmacokinetics, oral bioavailability, and metabolic profile of resveratrol and its dimethylether analog, pterostilbene, in rats*. *Cancer Chemotherapy and Pharmacology*, *68*(3), 593–601. https://doi.org/10.1007/s00280-010-1525-4.

Karu, N., Deng, L., Slae, M., Guo, A.C., Sajed, T., Huynh, H., … Wishart, D.S. (2018). *A review on human fecal metabolomics: Methods, applications and the human fecal metabolome database*. *Analytica Chimica Acta*, *1030*, 1–24. https://doi.org/10.1016/j.aca.2018.05.031.

Koh, Y.-C., Ho, C.-T., & Pan, M.-H. (2021). *Recent Advances in Health Benefits of Stilbenoids*. *Journal of Agricultural and Food Chemistry*, *69*(35), 10036–10057. https://doi.org/10.1021/acs.jafc.1c03699.

Lacalle-Bergeron, L., Portolés, T., López, F.J., Sancho, J.V., Ortega-Azorín, C., Asensio, E.M., … Corella, D. (2020). *Ultra-Performance Liquid Chromatography-Ion Mobility Separation-Quadruple Time-of-Flight MS (UHPLC-IMS-QTOF MS) metabolomics for short-term biomarker discovery of orange intake: A randomized, controlled crossover study*. *Nutrients*, *12*(7), 1916. https://doi.org/10.3390/nu12071916.

Lewinska, M., Santos-Laso, A., Arretxe, E., Alonso, C., Zhuravleva, E., Jimenez-Agüero, R., … Andersen, J.B. (2021). *The altered serum lipidome and its diagnostic potential for Non-Alcoholic Fatty Liver (NAFL)-associated hepatocellular carcinoma*. *EBioMedicine*, *73*, 103661. https://doi.org/10.1016/j.ebiom.2021.103661.

Maas, R. (2005). *Pharmacotherapies and their influence on asymmetric dimethylargine (ADMA)*. *Vascular Medicine*, *10*(2_suppl), S49–S57. https://doi.org/10.1191/1358863x05vm605oa.

Madatali Abuwani, A., Priyadarshini Dash, S., Ganesan, R., Renu, K., Vellingiri, B., Kandasamy, S., C.R., S. R., & Valsala Gopalakrishnan, A. (2021). Gut microbiome and metabolic response in non-alcoholic fatty liver disease. *Clinica Chimica Acta*, *523* (October), 304–314. doi:10.1016/j.cca.2021.10.014.

Mairinger, T., Causon, T.J., & Hann, S. (2018). The potential of ion mobility–mass spectrometry for non-targeted metabolomics. *Current Opinion in Chemical Biology*: *Vol. 42* (pp. 9–15). Elsevier Ltd. https://doi.org/10.1016/j.cbpa.2017.10.015.

Paglia, G., & Astarita, G. (2017). *Metabolomics and lipidomics using traveling-wave ion mobility mass spectrometry*. *Nature Protocols*, *12*(4), 797–813. https://doi.org/10.1038/nprot.2017.013.

Piras, C., Noto, A., Ibba, L., Deidda, M., Fanos, V., Muntoni, S., … Atzori, L. (2021). *Contribution of metabolomics to the understanding of NAFLD and NASH syndromes: A systematic review*. *Metabolites*, *11*(10), 694. https://doi.org/10.3390/metabo11100694.

Pirola, C.J., & Sookoian, S. (2018). *Multiomics biomarkers for the prediction of nonalcoholic fatty liver disease severity*. *World Journal of Gastroenterology*, *24*(15), 1601–1615. https://doi.org/10.3748/wjg.v24.i15.1601.

Schymanski, E.L., Jeon, J., Gulde, R., Fenner, K., Ruff, M., Singer, H.P., & Hollender, J. (2014). *Identifying small molecules via high resolution mass spectrometry: Communicating confidence*. *Environmental Science & Technology*, *48*(4), 2097–2098. https://doi.org/10.1021/es5002105.

Segers, K., Declerck, S., Mangelings, D., Heyden, Y.V., & Eeckhaut, A.V. (2019). *Analytical techniques for metabolomic studies: A review*. *Bioanalysis*, *11*(24), 2297–2318. https://doi.org/10.4155/bio-2019-0014.

Vergani, L., Baldini, F., Khalil, M., Voci, A., Putignano, P., & Miraglia, N. (2020). *New perspectives of S-adenosylmethionine (SAMe) applications to attenuate fatty acid-induced steatosis and oxidative stress in hepatic and endothelial cells*. *Molecules*, *25*(18), 4237. https://doi.org/10.3390/molecules25184237.

Vivanco, F., Barderas, M. G., Laborde, C. M., Posada, M., De La Cuesta, F., Zubiri, I., & Alvarez-Llamas, G. (2011). Metabolomic profiling for identification of novel potential biomarkers in cardiovascular diseases. *Journal of Biomedicine and Biotechnology* (Vol. 2011, pp. 1–9). doi:10.1155/2011/790132.

Wang, T.J., Larson, M.G., Vasan, R.S., Cheng, S., Rhee, E.P., McCabe, E., … Gerszten, R.E. (2011). *Metabolite profiles and the risk of developing diabetes*. *Nature Medicine*, *17*(4), 448–453. https://doi.org/10.1038/nm.2307.

Wolfender, J.-L., Marti, G., Thomas, A., & Bertrand, S. (2015). *Current approaches and challenges for the metabolite profiling of complex natural extracts*. *Journal of Chromatography A*, *1382*, 136–164. https://doi.org/10.1016/j.chroma.2014.10.091.

Worley, B., & Powers, R. (2012). *Multivariate analysis in metabolomics*. *Current*

Metabolomics, *1*(1), 92–107. https://doi.org/10.2174/2213235X130108.
Zhou, Z., Tu, J., Xiong, X., Shen, X., & Zhu, Z.-J. (2017). *LipidCCS: Prediction of collision cross-section values for lipids with high precision to support ion mobility–mass spectrometry-based lipidomics*. *Analytical Chemistry*, *89*(17), 9559–9566. https://doi.org/10.1021/acs.analchem.7b02625.
Zong, Z., Liu, J., Wang, N., Yang, C., Wang, Q., Zhang, W., … Deng, H. (2021). *Nicotinamide mononucleotide inhibits hepatic stellate cell activation to prevent liver fibrosis via promoting PGE2 degradation*. *Free Radical Biology and Medicine*, *162*(November 2020), 571–581. https://doi.org/10.1016/j.freeradbiomed.2020.11.014.